Properties of shape-driving orbitals: Rotational bands in ^{131}La

L. Hildingsson
Research Institute of Physics, S 104 05 Stockholm 50, Sweden

C. W. Beausang,* D. B. Fossan, R. Ma, E. S. Paul, W. F. Piel, Jr., and N. Xu
Department of Physics, State University of New York at Stony Brook, New York 11794
(Received 12 October 1988)

Several rotational bands have been populated in ^{131}La via the ^{116}Cd(^{19}F, $4n\gamma$) fusion-evaporation reaction. Bands built on low-lying $h_{11/2}$, $g_{7/2}$, and $d_{5/2}$ proton states have been identified. At higher spins, both proton and neutron $[h_{11/2}]^2$ alignments have been observed. While the proton alignment from low-Ω orbitals maintains a prolate nuclear shape, the alignment of high-Ω neutrons drives the nucleus to a collectively rotating oblate shape ($\gamma \sim -60°$). The results are interpreted in the framework of the cranked shell model. In addition, $B(M1;I\rightarrow I-1)/B(E2;I\rightarrow I-2)$ ratios have been extracted for several of the bands and the results compared to a semiclassical model to identify the detailed structure.

I. INTRODUCTION

The nuclei in the mass $A \sim 130$ region are known to be soft with respect to the triaxial deformation γ and are therefore sensitive to the γ-polarizing effects of specific quasiparticle configurations. This can lead to the coexistence of quadrupole structures of different spectroscopic character, which are determined by the configuration of the valence quasiparticles.[1-4] The polarizing effect is most pronounced for intruder high-j quasiparticles in the favored signature orbitals. When occupied, these orbitals tend to stabilize the nuclear shape around a specific γ value that is strongly dependent on the position of the Fermi surface within the high-j shell. In the light rare earth nuclei with mass $A \sim 130$, the proton Fermi surface lies in the lower $h_{11/2}$ midshell where the quasiparticle orbitals favor prolate axial symmetry. Thus odd-Z nuclei exhibit prolate $\pi h_{11/2}$ yrast bands. In addition, the alignment of a pair of protons tends to drive the nuclear shape towards $\gamma \geq 0°$ (Lund convention[5]). Conversely, the neutron Fermi surface lies in the upper $h_{11/2}$ midshell where the predicted deformation driving force is towards a collectively rotating oblate shape with $\gamma = -60°$. If the nucleus is soft with respect to γ, that is, if the potential energy difference V_{PO} between prolate and oblate shapes is sufficiently small, a neutron alignment will drive the nucleus to an oblate shape, and the nucleus will rotate collectively around an axis perpendicular to the symmetry axis.

In odd-A nuclei, the energy splitting between the two signature components of a given orbital is a sensitive probe of the triaxial deformation. A change in the γ deformation will usually manifest itself as a change in the signature splitting. For example, the odd-N nuclei[129,133]Ce and ^{135}Nd have a moderate signature splitting in their respective $\nu h_{11/2}$ yrast bands, which falls to zero when a pair of $h_{11/2}$ protons align.[6-8] This has been taken as evidence for a change in the nuclear deformation from a triaxial ($\gamma \leq 0°$) to a prolate shape caused by the γ-driving influence of the aligned proton orbitals.

A measurement of the signature splitting of the proton orbitals for odd-Z nuclei in this mass region can give similar information about the nuclear shape. Bands based on the $\pi h_{11/2}$ orbitals are expected to exhibit a large signature splitting for a prolate nuclear shape, whereas the splitting falls to zero when the nucleus adopts an oblate shape. Any observation of a decrease in the $h_{11/2}$ proton signature splitting can thus indicate a change in the triaxial deformation towards a negative γ value caused by the alignment of $h_{11/2}$ neutrons. Compared to the odd-N Ce and Nd isotopes, the resulting effect of a decrease in the signature splitting for odd-Z nuclei is caused by a large deformation change in the opposite direction in the (β,γ) plane (to more negative values of γ).

Electromagnetic properties are sensitive to the specific configurations and are thus useful in identifying band structures. Such properties are easily obtained for odd-A nuclei from the measured intensity ratios of competing $M1$ and $E2$ transitions. The observation of both $\Delta I = 1$ and $\Delta I = 2$ transitions in rotational bands allows the extraction of ratios of reduced transition probabilities

$$B(M1; I\rightarrow I-1)/B(E2; I\rightarrow I-2)$$

from measured branching ratios. The ratios can be compared with calculations for various quasiparticle configurations. Secondly, the sign of the $E2/M1$ mixing ratio δ for the $\Delta I = 1$ transitions is directly related to the sign of the quadrupole moment Q_0. By determining the mixing ratios for transitions within a rotational band of a known configuration, it is possible to determine the sign of the quadrupole moment and hence distinguish between prolate and oblate shapes.

The odd proton nucleus ^{131}La with 57 protons and 74 neutrons is expected to show several features that are characteristic of a soft rotor. Theoretical calculations

predict[3,9] the prolate-oblate energy difference V_{PO} to be small, and the nucleus therefore should be sensitive to the shape-polarizing effects of the valence quasiparticles. Although nuclei in this mass region are known to have predominantly prolate shapes, a soft nuclear core can lead to the occurrence of shape-coexistence phenomena.

From previous experiments[10] the ground state of ^{131}La is known to be $I^{\pi}=\frac{3}{2}^{(+)}$, and β decay studies[11–13] have identified several low-lying states including an $\frac{11}{2}^{-}$ isomer at 304 keV. In-beam investigations have revealed a rotational-like yrast band that has been interpreted[14,15] as based on an $h_{11/2}$ proton decoupled from a prolate core. Data from lifetime measurements indicate,[16] however, that triaxial deformation may be important.

The present paper presents a detailed study of the high spin level structure of ^{131}La. The study is a part of a systematic investigation of nuclei in the $A\sim130$ mass region undertaken at the State University of New York at Stony Brook. Section II presents the experimental procedures and Sec. III gives a detailed presentation of the level scheme. A comparison of the experimental results with cranked shell model (CSM) calculations is made in Sec. IV, and the electromagnetic properties are discussed in Sec. V. Preliminary results on this study have been published elsewhere.[17]

II. EXPERIMENTAL METHODS

High spin states of ^{131}La were populated by the ^{116}Cd(^{19}F,4n)^{131}La reaction. A cadmium target, consisting of 2.3 mg/cm^2 of ^{116}Cd (enriched to 96%) rolled onto a lead backing of thickness 50 mg/cm^2, was bombarded with a ^{19}F beam provided by the Stony Brook tandem-LINAC facility with typical beam intensities of a few particle nA. To determine the optimum beam energy, γ-ray excitation functions were studied at four different beam energies ranging from 76 to 90 MeV. The yield of previously known γ-ray transitions in ^{131}La (Refs. 14 and 15) was found to be an optimum at an energy $E_{\text{beam}}=76$ MeV. All of the subsequent measurements were there-

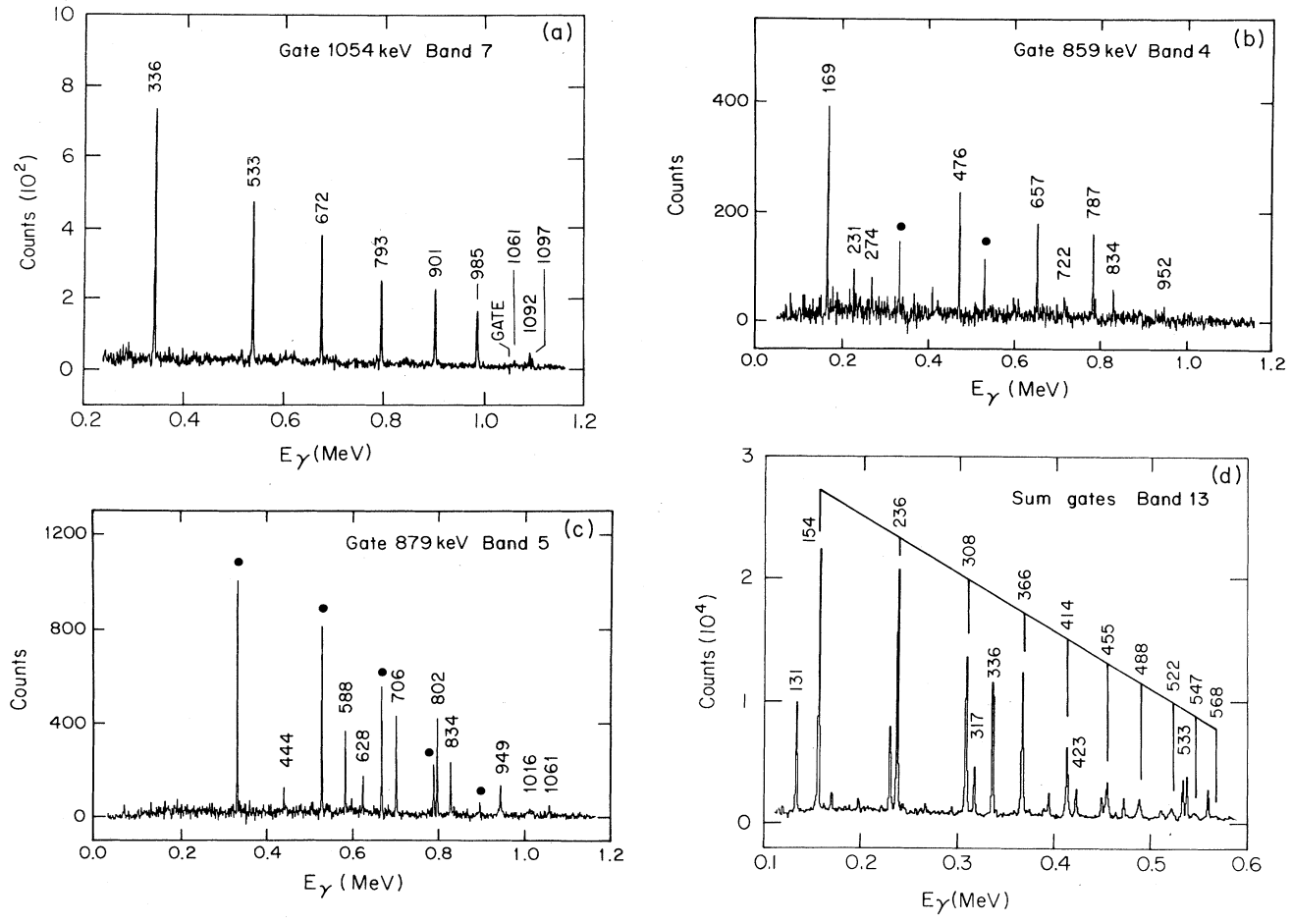

FIG. 1. Background subtracted gates set on transitions in ^{131}La. The γ rays are labeled with their energies in keV. (a) Gate set on the 1054-keV transition of the yrast $\pi h_{11/2}$ band 7. (b) Gate set on the 859-keV transition of band 4 based on a $\pi g_{7/2}$ orbital. Solid circles indicate transitions of the yrast band. (c) Gate set on the 879-keV transition of band 5 based on the $\pi g_{7/2}\otimes[\pi h_{11/2}]^2$ configuration. Solid circles indicate transitions of the yrast band. (d) Sum of gates set on the dipole transitions of band 13 based on the oblate $\pi h_{11/2}\otimes[\nu h_{11/2}]^2$ configuration.

TABLE I. Energies, intensities, and angular distribution data for the transitions assigned to ^{131}La which are shown in Fig. 2(a).

E_γ (keV)	I_γ^a	A_2/A_0	A_4/A_0	Assignment	Band[b]
109	120(5)			$\frac{11}{2}^- \rightarrow \frac{7}{2}^+$	7,4
118.8(2)[c]				$\frac{5}{2}^+ \rightarrow \frac{5}{2}^+$	1
145(1)				$\frac{5}{2}^+ \rightarrow \frac{3}{2}^+$	1
169.2(1)	136(3)	+0.04(4)	≡0.0	$\frac{7}{2}^+ \rightarrow \frac{5}{2}^+$	4,3
196.0(1)	19(1)[d]	+0.09(4)	≡0.0	$\frac{7}{2}^+ \rightarrow \frac{3}{2}^+$	4
231.0(2)	2.1(1)	0.0(1)	≡0.0	$\frac{11}{2}^+ \rightarrow \frac{9}{2}^+$	4,3
244.8(1)	3.4(1)[d]			$\frac{9}{2}^+ \rightarrow \frac{7}{2}^+$	3,4
265.8(3)				$(\frac{13}{2}^-) \rightarrow \frac{15}{2}^-$	8,7
273.9(2)	0.5(1)[d]			$\frac{15}{2}^+ \rightarrow \frac{13}{2}^+$	4,3
284.2(4)	0.4(1)[d]			$\frac{31}{2}^+ \rightarrow \frac{29}{2}^+$	5,6
307.4(4)	0.4(1)[d]			$\frac{19}{2}^+ \rightarrow \frac{17}{2}^+$	4,3
336.1(1)	≡100	+0.36(3)	−0.15(4)	$\frac{15}{2}^- \rightarrow \frac{11}{2}^-$	7
383.5(2)	0.9(1)[d]			$\frac{13}{2}^+ \rightarrow \frac{11}{2}^+$	3,4
392.7(2)	2.6(1)	−0.60(6)	+0.10(6)	$\frac{9}{2}^+ \rightarrow \frac{7}{2}^+$	1,4
395.3(5)				$\frac{7}{2}^+ \rightarrow \frac{5}{2}^+$	2,3
396(1)				$(\frac{17}{2}^- \rightarrow \frac{15}{2}^-)$	10,9
398.0(4)	0.6(2)[d]			$\frac{35}{2}^+ \rightarrow \frac{33}{2}^+$	5,6
403.4(2)	0.8(1)[d]	−0.01(6)	≡0.0	$\frac{33}{2}^+ \rightarrow \frac{31}{2}^+$	6,5
414.3(1)	8.4(2)			$\frac{9}{2}^+ \rightarrow \frac{5}{2}^+$	3
421.5(2)	1.3(1)	0.0(1)	≡0.0	$\frac{29}{2}^+ \rightarrow \frac{27}{2}^+$	6,5
422.1(3)				$(\frac{21}{2}^- \rightarrow \frac{19}{2}^-)$	10,9
422.5(5)				$\frac{7}{2}^+ \rightarrow \frac{3}{2}^+$	2
435(1)	0.3(1)[d]			$\frac{37}{2}^+ \rightarrow \frac{35}{2}^+$	6,5
442.9(2)	5.3(1)			$\frac{9}{2}^+ \rightarrow \frac{5}{2}^+$	1
444.3(1)	2.2(1)	+0.01(7)	≡0.0	$\frac{23}{2}^+ \rightarrow \frac{19}{2}^+$	5
449.9(3)				$(\frac{15}{2}^- \rightarrow \frac{13}{2}^-)$	9,8
466.4(3)	6.9(2)	−0.05(4)	≡0.0	$\frac{25}{2}^+ \rightarrow \frac{23}{2}^+$	6,5
476.1(1)	6.8(2)	+0.07(4)	≡0.0	$\frac{11}{2}^+ \rightarrow \frac{7}{2}^+$	4
479.9(3)	0.4(1)[d]			$\frac{17}{2}^+ \rightarrow \frac{15}{2}^+$	3,4
480.7(3)					
522.6(3)	1.4(7)[d]			$(\frac{19}{2}^- \rightarrow \frac{17}{2}^-)$	9,8
525(1)				$\frac{21}{2}^+ \rightarrow \frac{19}{2}^+$	3,4
529.9(3)				$(\frac{23}{2}^- \rightarrow \frac{21}{2}^-)$	9,8
530.5(3)				$\rightarrow \frac{19}{2}^-$	
533.5(1)	70(1)	+0.36(3)	−0.22(4)	$\frac{19}{2}^- \rightarrow \frac{15}{2}^-$	7
543.3(1)	2.9(2)[d]			$\frac{29}{2}^+ \rightarrow \frac{25}{2}^+$	6
548(1)	<0.2[d]			$(\frac{31}{2}^- \rightarrow \frac{29}{2}^-)$	9,8
551.1(3)	0.4(2)[d]			$(\frac{27}{2}^- \rightarrow \frac{25}{2}^-)$	9,8
577.0(3)	0.3(2)[d]			$(\frac{35}{2}^-) \rightarrow \frac{35}{2}^-$	9,7
583.6(3)	1.1(6)[d]			$\rightarrow \frac{15}{2}^-$	
584.0(5)				$(\frac{11}{2}^+) \rightarrow \frac{9}{2}^+$	2,3
588.0(1)	7.2(2)	+0.18(4)	−0.15(5)	$\frac{27}{2}^+ \rightarrow \frac{23}{2}^+$	5
602.0(3)				$(\frac{13}{2}^-) \rightarrow \frac{11}{2}^-$	8,7
602.8(5)				$(\frac{11}{2}^+) \rightarrow \frac{7}{2}^+$	2
614.9(1)	7.6(2)	+0.10(5)	≡0.0	$\frac{13}{2}^+ \rightarrow \frac{9}{2}^+$	3

TABLE I. (*Continued.*)

E_γ (keV)	I_γ^a	A_2/A_0	A_4/A_0	Assignment	Band[b]
628.4(2)	3.4(1)	+0.30(7)	≡0.0	$\frac{27}{2}^+ \rightarrow \frac{27}{2}^-$	5,7
637.7(2)	5(1)[d]			$(\frac{13}{2}^+) \rightarrow \frac{9}{2}^+$	1
650.1(3)	0.8(4)[d]			$(\frac{21}{2}^- \rightarrow)$	10
657.3(1)	3.4(1)	+0.22(6)	+0.05(7)	$\frac{15}{2}^+ \rightarrow \frac{11}{2}^+$	4
672.0(1)	56(1)	+0.35(3)	−0.14(4)	$\frac{23}{2}^- \rightarrow \frac{19}{2}^-$	7
680.3(3)				$(\frac{21}{2}^- \rightarrow \frac{17}{2}^-)$	8
687.6(3)				$(\frac{23}{2}^- \rightarrow \frac{19}{2}^-)$	9
687.8(1)	6.3(2)[d]	+0.27(5)	≡0.0	$\frac{33}{2}^+ \rightarrow \frac{29}{2}^+$	6
690.0(3)				$(\frac{31}{2}^-) \rightarrow \frac{31}{2}^-$	9,7
706.0(1)	11.3(3)	+0.18(5)	≡0.0	$\frac{31}{2}^+ \rightarrow \frac{27}{2}^+$	5
715.8(3)				$(\frac{15}{2}^-) \rightarrow \frac{15}{2}^-$	9,7
722.1(2)	0.3(1)[d]			$(\frac{31}{2}^+ \rightarrow \frac{27}{2}^+)$	4
728(1)				$(\frac{15}{2}^+ \rightarrow \frac{11}{2}^+)$	2
751(1)				$\frac{13}{2}^+ \rightarrow \frac{11}{2}^-$	3,7
753.9(1)	3.1(1)	+0.32(6)	−0.07(7)	$\frac{17}{2}^+ \rightarrow \frac{13}{2}^+$	3
757.5(3)	0.5(3)[d]			$(\frac{25}{2}^- \rightarrow \frac{21}{2}^-)$	8
760.0(3)	0.6(3)[d]			$(\frac{27}{2}^-) \rightarrow \frac{27}{2}^-$	9,7
763.6(3)	1.2(6)[d]			$(\frac{25}{2}^- \rightarrow \frac{21}{2}^-)$	10
770.0(3)	4.7(4)[d]			$(\frac{17}{2}^-) \rightarrow \frac{15}{2}^-$	8,7
771.3(2)	3(1)[d]			$(\frac{17}{2}^+ \rightarrow \frac{13}{2}^+)$	1
774(1)	0.6(3)[d]			$(\frac{23}{2}^-) \rightarrow \frac{23}{2}^-$	9,7
778(1)	1.0(5)[d]			$(\frac{27}{2}^- \rightarrow \frac{23}{2}^-)$	9
787.2(2)	2.6(1)	+0.02(8)	≡0.0	$\frac{19}{2}^+ \rightarrow \frac{15}{2}^+$	4
793.2(1)	32(1)	+0.32(3)	−0.12(4)	$\frac{27}{2}^- \rightarrow \frac{23}{2}^-$	7
801.8(1)	7.6(2)[d]	+0.35(6)	≡0.0	$\frac{35}{2}^+ \rightarrow \frac{31}{2}^+$	5
831.5(3)				$(\frac{31}{2}^- \rightarrow \frac{27}{2}^-)$	9
832.0(2)	1.3(1)[d]			$\frac{21}{2}^+ \rightarrow \frac{17}{2}^+$	3
833.6(3)	16.5(3)	+0.31(4)	≡0.0	$\frac{37}{2}^+ \rightarrow \frac{33}{2}^+$	6
833.7(2)				$\frac{23}{2}^+ \rightarrow \frac{23}{2}^-$	5,7
834.0(2)	0.7(1)[d]			$(\frac{27}{2}^+) \rightarrow \frac{23}{2}^+$	4
834.1(3)				$(\frac{29}{2}^- \rightarrow \frac{25}{2}^-)$	8
837(1)				$\frac{33}{2}^+ \rightarrow \frac{31}{2}^-$	6,7
844(1)	0.3(1)[d]			$\rightarrow \frac{21}{2}^+$	3
845(1)				$(\frac{17}{2}^- \rightarrow \frac{13}{2}^-)$	10,8
848(1)	<1.0			$(\frac{21}{2}^+ \rightarrow \frac{17}{2}^+)$	1
859.0(2)	0.9(1)	+0.5(2)	0.0(2)	$\frac{23}{2}^+ \rightarrow \frac{19}{2}^+$	4
870(1)				$(\frac{29}{2}^- \rightarrow \frac{25}{2}^-)$	10
873.2(3)	0.7(4)[d]			$(\frac{35}{2}^- \rightarrow \frac{31}{2}^-)$	9
878.8(1)	2.8(1)	+0.47(8)	−0.09(9)	$\frac{39}{2}^+ \rightarrow \frac{35}{2}^+$	5
897(1)				$(\frac{33}{2}^- \rightarrow \frac{29}{2}^-)$	8
901.5(1)	15(1)	+0.44(5)	−0.33(6)	$\frac{31}{2}^- \rightarrow \frac{27}{2}^-$	7
905(1)				$\rightarrow \frac{21}{2}^+$	3
916.6(3)	1.5(8)[d]			$(\frac{21}{2}^-) \rightarrow \frac{19}{2}^-$	8,7
928.5(3)	1.6(1)	+0.2(1)	−0.2(1)	$\frac{41}{2}^+ \rightarrow \frac{37}{2}^+$	6
944.5(3)				$(\frac{21}{2}^- \rightarrow \frac{17}{2}^-)$	10,8

TABLE I. (*Continued.*)

E_γ (keV)	I_γ^a	A_2/A_0	A_4/A_0	Assignment	Band[b]
948.5(3)				$\frac{43}{2}^+ \rightarrow \frac{39}{2}^+$	5
952(1)				$\rightarrow \frac{23}{2}^+$	4
985.7(1)	6.2(2)[d]	+0.25(5)	−0.01(6)	$\frac{35}{2}^- \rightarrow \frac{31}{2}^-$	7
1002.1(3)	1.5(8)[d]			$(\frac{25}{2}^-) \rightarrow \frac{23}{2}^-$	8,7
1010(1)				$\frac{45}{2}^+ \rightarrow \frac{41}{2}^+$	6
1016(1)				$\frac{47}{2}^+ \rightarrow \frac{43}{2}^+$	5
1028(1)	0.3(2)[d]			$(\frac{25}{2}^- \rightarrow \frac{21}{2}^-)$	10,8
1040(1)	0.5(3)[d]			$(\frac{33}{2}^-) \rightarrow \frac{31}{2}^-$	8,7
1043.0(3)	1.1(6)[d]			$(\frac{29}{2}^-) \rightarrow \frac{27}{2}^-$	8,7
1049.1(3)				$\frac{29}{2}^+ \rightarrow \frac{27}{2}^-$	6,7
1053(1)				$(\frac{15}{2}^-) \rightarrow \frac{11}{2}^-$	9,7
1054.6(2)	2.7(2)[d]			$\frac{39}{2}^- \rightarrow \frac{35}{2}^-$	7
1061.2(2)				$\frac{19}{2}^+ \rightarrow \frac{19}{2}^-$	5,7
1061.6(4)	0.6(1)[d]	+0.48(11)	−0.15(13)	$\frac{47}{2}^- \rightarrow \frac{43}{2}^-$	7
1092.4(3)	0.8(2)[d]			$\frac{43}{2}^- \rightarrow \frac{39}{2}^-$	7
1097.1(4)	0.4(2)[d]			$\frac{51}{2}^- \rightarrow \frac{47}{2}^-$	7
1142(1)	<0.2			$\frac{55}{2}^- \rightarrow \frac{51}{2}^-$	7
1169(1)	<0.2[d]			$\frac{17}{2}^+ \rightarrow \frac{15}{2}^-$	3,7
1293.2(5)	1.1(6)[d]			$(\frac{19}{2}^-) \rightarrow \frac{15}{2}^-$	9,7
1299.2(3)	2.2(1)	−0.36(8)	≡0.0	$\frac{25}{2}^+ \rightarrow \frac{23}{2}^-$	6,7
1446.8(5)	1.0(5)[d]			$(\frac{23}{2}^-) \rightarrow \frac{19}{2}^-$	9,7
1553.8(5)	0.6(3)[d]			$(\frac{27}{2}^-) \rightarrow \frac{23}{2}^-$	9,7

[a]The intensities are normalized to the 336.1-keV $\frac{15}{2}^- \rightarrow \frac{11}{2}^-$ transition.
[b]The band numbers refer to the labels in Fig. 2(a). A single number indicates an in-band transition, while two numbers indicate an interband transition.
[c]Doublet with a strong transition in ^{130}La.
[d]Intensity obtained from coincidence data.

fore undertaken at this energy.

The γ-γ coincidence data were recorded with four n-type Ge detectors, each having an efficiency of 25% relative to a 7.6-cm×7.6-cm NaI(Tl) detector for 1.33-MeV γ rays. The detectors were located at ±57° and ±132° with respect to the beam direction, and at a distance of 14 cm from the target. Each of the four detectors was surrounded by a bismuth germanate (BGO) anti-Compton shield of the transverse type.[18] The coincidence resolution time 2τ for the Ge detectors was set to 100 ns. Approximately 30 million twofold, or higher-order, events were recorded onto magnetic tape for subsequent off-line analysis; the data were sorted into a two-dimensional array of E_γ vs E_γ. Examples of background subtracted gated spectra, generated from this array, are presented in Fig. 1.

In order to obtain information about the multipolarity of the transitions assigned to ^{131}La, a γ-ray angular distribution measurement was undertaken using four different angles. Data were taken simultaneously with the four detectors placed 22 cm from the target and at angles 0, 90, 130, and 150° with respect to the beam direction. A ^{152}Eu source placed at the target position, together with beam-spot activity (beam off), were used for normalization of the four detectors. The measured γ-ray intensities were then fitted to the formula

$$W(\theta) = A_0 + A_2 P_2(\cos\theta) + A_4 P_4(\cos\theta) ,$$

where θ is the detector angle, $P_2(\cos\theta)$ and $P_4(\cos\theta)$ are Legendre polynomials, and A_0, A_2, and A_4 are adjustable parameters. The results are presented in Tables I and II, where a small correction has been made to each A_2/A_0 and A_4/A_0 value to adjust for the finite detector size.

A pulsed-beam–γ measurement was performed to search for isomeric states. The ^{19}F beam was pulsed with a 424-ns repetition period. The γ rays were detected in a coaxial Ge(Li) detector positioned at 90°. In this way, half-lives in the range of 8–400 ns could be studied.

III. THE LEVEL SCHEME OF ^{131}La

The level scheme of ^{131}La obtained from the present work is shown in Figs. 2(a) and (b). The levels have been

TABLE II. Energies, intensities, and angular distribution data for the transitions assigned to ^{131}La which are shown in Fig. 2(b).

E_γ (keV)	I_γ^a	A_2/A_0	A_4/A_0	Assignment	Band[b]
67.3(6)				$(\frac{21}{2}^- \rightarrow \frac{19}{2}^-)$	13
78(1)				$(\frac{17}{2}^+ \rightarrow \frac{15}{2}^+)$	15
131.6(1)	13.2(3)	−0.08(4)	≡0.0	$(\frac{19}{2}^- \rightarrow \frac{17}{2}^+)$	13,15
152.1(3)				$(\frac{19}{2}^+ \rightarrow \frac{17}{2}^+)$	15
154.3(1)	10.1(2)	−0.37(5)	≡0.0	$(\frac{23}{2}^- \rightarrow \frac{21}{2}^-)$	13
182.6(3)				$(\frac{21}{2}^+ \rightarrow \frac{19}{2}^+)$	15
234.8(3)				$\rightarrow(\frac{21}{2}^+)$	14,15
236.1	8.4(2)	−0.40(4)	≡0.0	$(\frac{25}{2}^- \rightarrow \frac{23}{2}^-)$	13
242.0(3)					
261.3(3)				$(\frac{23}{2}^+ \rightarrow \frac{21}{2}^+)$	15
267.4(3)	1.8[c]				11
301.0(3)				$(\frac{23}{2}^+) \rightarrow \frac{21}{2}^+$	15,3
308.2(1)	6.3(2)	−0.45(4)	≡0.0	$(\frac{27}{2}^- \rightarrow \frac{25}{2}^-)$	13
315(1)				$(\frac{15}{2}^+) \rightarrow$	15
317.3(1)	1.6(8)[c]			$(\frac{19}{2}^-) \rightarrow$	13
331.5(3)					14
341.7(3)	2(1)[c]				11
345.0(3)				$\rightarrow(\frac{23}{2}^+)$	14,15
366.6(1)	3.6(1)	−0.54(4)	≡0.0	$(\frac{29}{2}^- \rightarrow \frac{27}{2}^-)$	13
371.4(3)	0.6(3)[c]				11
371.5(3)					14
389.9(7)	1.0(1)[c]			$(\frac{25}{2}^- \rightarrow \frac{21}{2}^-)$	13
394.6(3)	1.2(6)[c]			$(\frac{17}{2}^+) \rightarrow$	15
409.6(3)	1.6(8)[c]				11
413.9(1)	2.6(1)[c]	−0.15(4)	≡0.0	$(\frac{31}{2}^- \rightarrow \frac{29}{2}^-)$	13
423.5(1)	2.5(1)	+0.38(1)	+0.06(1)	$(\frac{21}{2}^-) \rightarrow \frac{21}{2}^-$	13,12
427.1(3)				$(\frac{25}{2}^+ \rightarrow \frac{23}{2}^+)$	15
427.5(2)				$(\frac{23}{2}^-) \rightarrow \frac{21}{2}^-$	12
455.4(3)	1.5(2)	−0.46(2)	≡0.0	$(\frac{33}{2}^- \rightarrow \frac{31}{2}^-)$	13
458.7(3)	0.7(4)[c]				11
469.3(2)				$(\frac{25}{2}^- \rightarrow \frac{23}{2}^-)$	12
472.7(3)					
472.8(3)	1.7(9)[c]			$\rightarrow(\frac{31}{2}^-)$	11,9
480.7(3)	0.8[c]				11
488.6(3)	1.0(1)[c]			$(\frac{35}{2}^- \rightarrow \frac{33}{2}^-)$	13
507(1)	< 1.2[c]				11
509(1)				$(\frac{27}{2}^- \rightarrow \frac{25}{2}^-)$	12
522.2(3)	0.6(1)[c]	0.6(1)[c]		$(\frac{37}{2}^- \rightarrow \frac{35}{2}^-)$	13
537.8(3)				$\rightarrow(\frac{13}{2}^-)$	
544.1(6)	0.5(1)[c]			$(\frac{27}{2}^- \rightarrow \frac{23}{2}^-)$	13
547.8(5)	0.3(1)[c]			$(\frac{39}{2}^- \rightarrow \frac{37}{2}^-)$	13
559.5(5)				$(\frac{19}{2}^-) \rightarrow$	13
559.8(3)				$\rightarrow \frac{15}{2}^-$	
564(1)				$(\frac{21}{2}^+) \rightarrow \frac{19}{2}^+$	15,4
568.5(6)				$(\frac{41}{2}^- \rightarrow \frac{39}{2}^-)$	13
579(1)				$(\frac{43}{2}^- \rightarrow \frac{41}{2}^-)$	13

TABLE II. (*Continued*).

E_γ (keV)	I_γ^a	A_2/A_0	A_4/A_0	Assignment	Band[b]
580.2(3)				$(\frac{19}{2}^+)\rightarrow$	15
675.6(4)	0.5(1)[c]			$(\frac{29}{2}^- \rightarrow \frac{25}{2}^-)$	13
703.8(3)					14
711.3(2)	2(1)[c]			$(\frac{21}{2}^- \rightarrow \frac{17}{2}^-)$	12,8
727.8(3)				$(\frac{25}{2}^+)\rightarrow \frac{21}{2}^+$	15,3
749.4(2)	0.8(2)[c]			$\rightarrow(\frac{17}{2}^-)$	
756(1)					14
780.7(4)	0.4(1)[c]			$(\frac{31}{2}^- \rightarrow \frac{27}{2}^-)$	13
869.8(5)	0.4(1)[c]			$(\frac{33}{2}^- \rightarrow \frac{29}{2}^-)$	13
871.8(3)				$(\frac{21}{2}^+)\rightarrow \frac{17}{2}^+$	15,3
896(1)				$(\frac{25}{2}^-)\rightarrow \frac{21}{2}^-$	12
900.9(3)				$(\frac{17}{2}^+)\rightarrow$	15
941.0(3)	3(1)[c]			$\rightarrow \frac{27}{2}^-$	11,7
943.9(7)	0.2(1)[c]			$(\frac{35}{2}^- \rightarrow \frac{31}{2}^-)$	13
947.6(1)	7(1)	−0.42(4)	≡0.0	$\frac{21}{2}^- \rightarrow \frac{19}{2}^-$	12,7
978(1)				$(\frac{27}{2}^- \rightarrow \frac{23}{2}^-)$	12
988.8(3)				$(\frac{17}{2}^+ \rightarrow \frac{15}{2}^-)$	15,9
1010(1)	<0.1[c]			$(\frac{37}{2}^- \rightarrow \frac{33}{2}^-)$	13
1011.1(3)				$\rightarrow(\frac{13}{2}^-)$	
1015.1(3)	4(2)[c]			$\rightarrow \frac{27}{2}^-$	11,7
1069(1)	<0.1[c]			$(\frac{39}{2}^- \rightarrow \frac{35}{2}^-)$	13
1115(1)				$(\frac{41}{2}^- \rightarrow \frac{37}{2}^-)$	13
1140.7(3)				$\rightarrow \frac{11}{2}^-$	
1171.4(4)	0.4(2)[c]			$(\frac{17}{2}^+)\rightarrow \frac{19}{2}^-$	15,7
1310.2(4)	2(1)[c]			$\rightarrow \frac{15}{2}^-$	
1361.6(5)				$(\frac{15}{2}^+ \rightarrow \frac{13}{2}^-)$	15,8
1506.8(5)				$(\frac{21}{2}^+)\rightarrow \frac{19}{2}^-$	15,7
1734.8(5)	2(1)[c]			$\rightarrow \frac{23}{2}^-$	11,7
1742.5(5)	1.0(5)[c]			$\rightarrow \frac{27}{2}^-$	11,7

[a]The intensities are normalized to the 336.1-keV $\frac{15}{2}^- \rightarrow \frac{11}{2}^-$ transition.

[b]The band numbers refer to the labels in Fig. 2(b). A single number indicates an in-band transition, while two numbers indicate an interband transition.

[c]Intensity obtained from coincidence data.

arranged into several bands labeled 1–15 in order to facilitate the discussion. The ordering of the γ rays has been determined by their coincidence relationships and their relative intensities. For some weak transitions, the placement in the level scheme is uncertain and these transitions are shown dashed.

The properties of the γ rays assigned to ^{131}La are listed in Tables I and II together with their placement in the level scheme. For the weaker transitions, the γ-ray intensities have been obtained from the coincidence data. Since the coincidence data are averaged over all six possible pairs of the four detectors, any angular correlation effects are expected to be small. The spin and parity assignments of the levels are based on the multipolarities of the transitions deduced from the angular distribution coefficients A_2/A_0 and A_4/A_0. Several tentative assignments, within parentheses, have been made for the weak γ rays and are based on systematic rotational properties.

In the positive parity bands 1–4, the first few transitions at low excitation energy were previously known from studies of the decay of ^{131}Ce (Refs. 11 and 13). The 26-keV transition from the bottom of band 3 to the ground state was not detected in our experiment since it is below the energy thresholds of the electronics. The spin and parity assignments of band 1 are based on the multipolarity of the 392.7-keV transition. The large negative A_2/A_0 coefficient implies a mixed $M1+E2$ transition; thus $I^\pi=\frac{9}{2}^+$ has been assigned to the state at 588

keV and, consequently, $I^{\pi}=\frac{5}{2}^{+}$ to the state at 145 keV. A comparison with the isotope ^{133}La, where a similar band has been found built on a second $\frac{5}{2}^{+}$ state,[19] supports this assignment. The states of bands 1–4 decay mainly by in-band $E2$ transitions, but weak $\Delta I=1$ interband transitions connect bands 3 and 4.

Bands 5 and 6 form two sequences of stretched ($\Delta I=2$) $E2$ transitions connected by weaker $\Delta I=1$ tran-

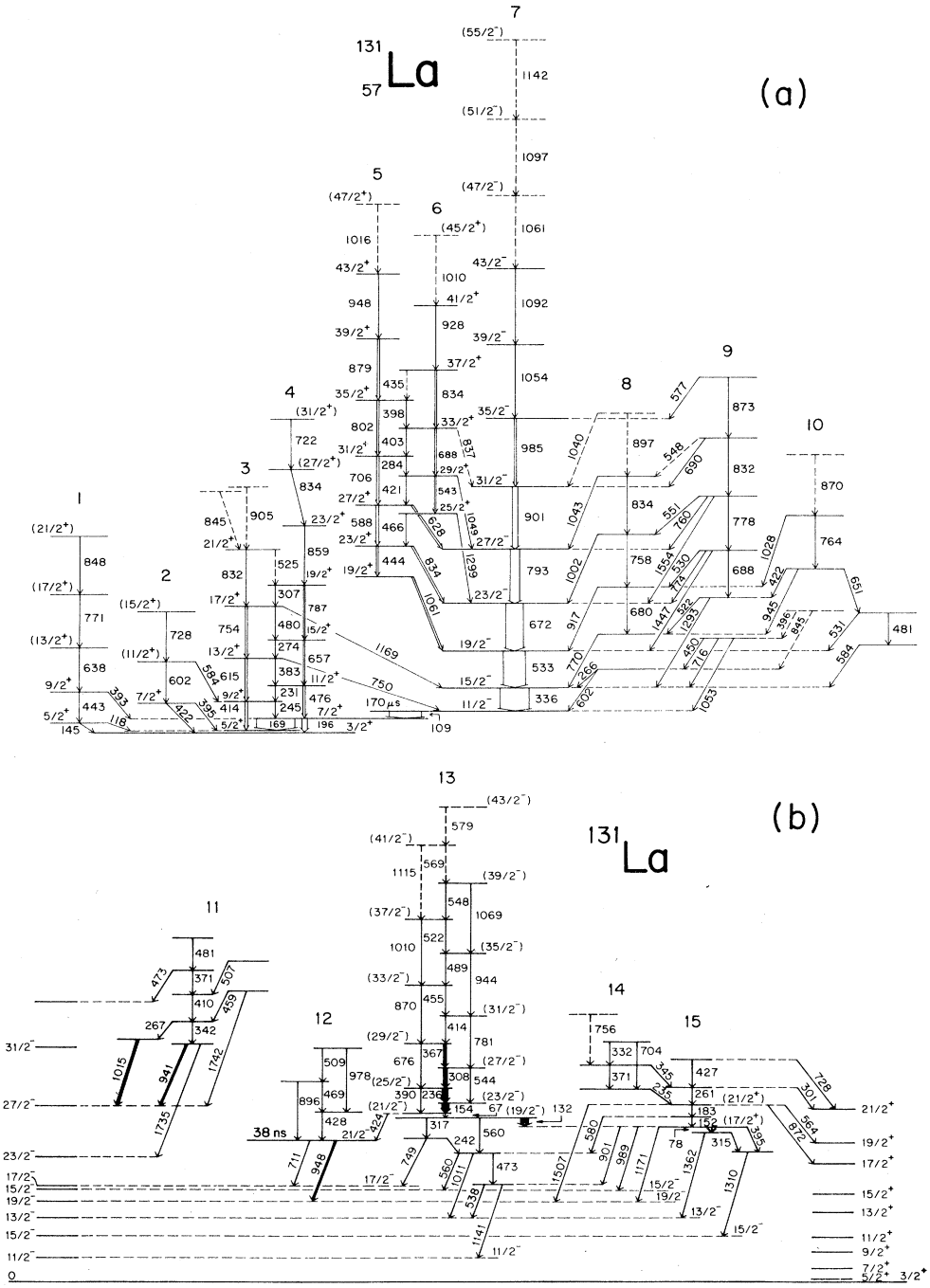

FIG. 2. (a) Portion of the level scheme of ^{131}La, deduced from this work, showing the prolate bands. The γ-ray energies are given in keV, and the thickness of the arrows represents the γ-ray intensity following the 76-MeV bombardment. Not all tentative spin-parity assignments are included. (b) Remainder of the level scheme of ^{131}La including, to the left, prolate negative-parity states and, to the right, prolate positive-parity states.

sitions. The spin assignments for the bands are based on the nonstretched ($\Delta I=0$) 628.4-keV transition and the stretched ($\Delta I=1$) 1299.2-keV dipole transition into the $\frac{27}{2}^-$ and $\frac{23}{2}^-$ yrast states, respectively. Bands showing similar properties (energies, bandhead spins, and decay patterns) have been reported in other odd-proton nuclei in this mass region, where a positive parity assignment has been established from measurements of the conversion coefficients[20] or the linear polarization.[21] We therefore adopt a positive-parity assignment for bands 5 and 6.

The negative-parity band 7, previously known up to $I^\pi=\frac{27}{2}^-$, has now been extended up to $I^\pi=(\frac{55}{2}^-)$. The top three transitions of this band are dashed in Fig. 2(a) since their ordering is not certain. Since the band is yrast, it is strongly populated in the reaction. The half-life of the $\frac{11}{2}^-$ isomer was measured[12] in a previous experiment to be $t_{1/2}=170$ μs. Because of the long half-life, no coincidences were observed between those transitions occurring above and below this isomer.

Bands 8–10 were only weakly populated in the present experiment; therefore, information on the multipolarity of the transitions could only be obtained in a few cases. Because of the observed systematic multipole decay branches to several bands including the yrast band, a consistent set of negative-parity levels is defined for these $\Delta I=2$ bands. The corresponding tentative I^π assignments for these bands are shown in Table I. A characteristic feature of these three bands is that the intensity of the in-band $E2$ transition from each level is weak compared to that of the dipole transition branching out of the band. For this reason the lowest in-band $E2$ transitions were not observed. The bandheads interpreted from the data for bands 8, 9, and 10 have $I^\pi=(\frac{13}{2}^-)$, $(\frac{15}{2}^-)$, and $(\frac{17}{2}^-)$, respectively. Band 8 connects to the yrast band at each level by transitions that are consistent with stretched dipoles. The characteristic decay pattern out of band 9 involves stretched $E2$ and $\Delta I=0$ dipole transitions to the yrast band as well as stretched dipole transitions to band 8.

A weakly populated band, labeled 12 in Fig. 2(b), was found built on an isomeric state at 2121 keV. From the pulsed beam experiment, a half-life of 38±2 ns was determined for this state. The negative A_2/A_0 coefficient listed in Table II for the 947.6-keV transition implies that it

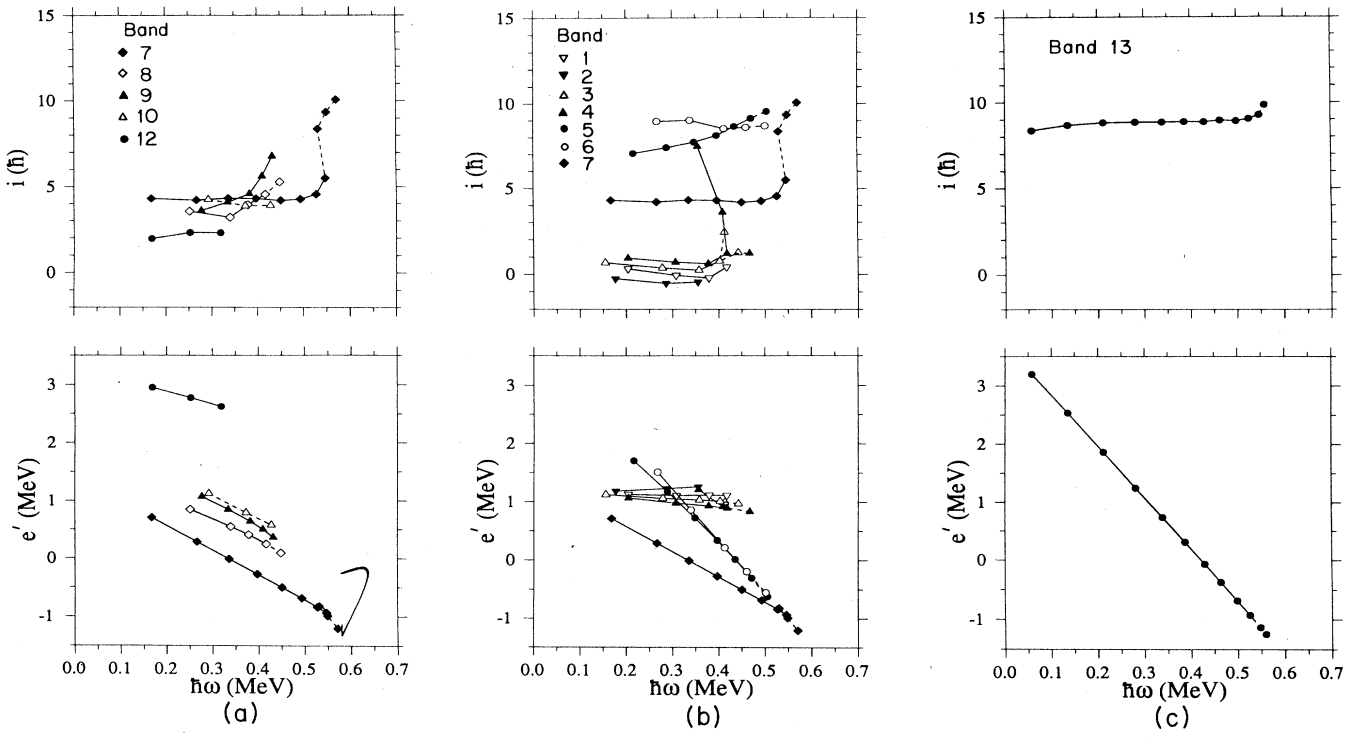

FIG. 3. (a) Experimental alignments (top) and Routhians (bottom) for the negative-parity prolate bands in ^{131}La. The reference configuration is given by $\mathcal{J}_{\rm ref}=14.7+45.8\omega^2$ ($\hbar^2$ MeV^{-1}). The two signatures of the $\pi h_{11/2}$ configuration (bands 7 and 8) are indicated by the diamonds, while the other two negative-parity bands (9 and 10) are given by the triangles; open symbols are for signature $\alpha=+\frac{1}{2}$, and solid are for $\alpha=-\frac{1}{2}$. The solid circles indicate the band (possibly oblate) built on the isomeric $\frac{21}{2}^-$ state (band 12). (b) Same as (a) but for the positive-parity bands. Both signatures of the $\pi g_{7/2}$ configuration (bands 3 and 4) are indicated by the up triangles (open: $\alpha=-\frac{1}{2}$, solid: $\alpha=+\frac{1}{2}$), while both signatures of the $\pi d_{5/2}$ configuration (bands 1 and 2) are indicated by the down triangles (open: $\alpha=+\frac{1}{2}$, solid: $\alpha=-\frac{1}{2}$). The two signatures of the $\pi g_{7/2}\otimes[\pi h_{11/2}]^2$ configuration (bands 5 and 6) are given by the circles (open: $\alpha=+\frac{1}{2}$, solid: $\alpha=-\frac{1}{2}$). The yrast $\pi h_{11/2}$ band 7 is included for comparison (solid diamonds). (c) Same as (a) but for the oblate $\pi h_{11/2}\otimes[\nu h_{11/2}]^2$ band 13. The reference configuration is here given by $\mathcal{J}_{\rm ref}=9.9+30.7\omega^2$ ($\hbar^2$ MeV^{-1}) (see text).

is of $\Delta I=1$ character, and therefore a spin of $\frac{21}{2}$ is inferred for the isomeric state. The weak branching to the $\frac{17}{2}^-$ state implies a negative parity if an $E2$ multipolarity is assumed. The regular pattern of this band suggests that it is a sequence of $\Delta I=1$ transitions with weaker $E2$ crossovers.

A second $\Delta I=1$ band, labeled 13 in Fig. 2(b), could be followed up to high spins. The large negative A_2/A_0 coefficients in the angular distribution data imply mixed $M1+E2$ transitions with an $E2/M1$ mixing ratio $\delta<0$. The $E2$ crossover transitions were only weakly observed. The 67-keV transition feeding the bandhead at 2476 keV was just above the energy threshold of the electronics, and therefore its intensity could not be measured. However, a consideration of the intensity balance shows that the decay goes mainly through this transition and stays within the band. At the bandhead the decay branches out to several intermediate states before feeding into the negative-parity yrast band. The 423.5-keV transition, connecting the band with the $\frac{21}{2}^-$ isomer, has angular distribution coefficients consistent with a nonstretched ($\Delta I=0$) dipole or stretched ($\Delta I=2$) quadrupole transition giving a spin of $\frac{19}{2}$ or $\frac{23}{2}$ for the bandhead, respectively. A consideration of the other decay paths supports the $\frac{19}{2}$ assignment. This assignment differs from that of the previous work[17] but does not change the interpretation of the band. A tentative negative-parity assignment is inferred from possible quasiparticle configurations (see Sec. IV C below).

Bands 11, 14, 15 do not form any regular rotational band structures. The decay of the lowest state of band 11 feeds the $\frac{23}{2}^-$ and $\frac{27}{2}^-$ states of the yrast band. This suggests a spin of $\frac{25}{2}$ of $\frac{27}{2}$ for this state. Band 15 feeds both yrast negative-parity states and states in the positive-parity bands 3 and 4. Considering the decay paths, a possible spin and parity assignment of the first level of band 15 at 2345 keV is $\frac{17}{2}^+$.

Several additional states at low spin could be identified. These are also shown in Fig. 2(b). Besides the $\frac{21}{2}^-$ isomeric state, no other states with half-lives in the range 8–400 ns were observed.

IV. ROUTHIANS AND ALIGNMENTS

In order to discuss the rotational properties of this nucleus, it is convenient to transform the data to the intrinsic body-fixed coordinate system. This has been achieved following the description outlined by Bengtsson and Frauendorf,[22] and the results are presented in Figs. 3(a)–(c). The experimental alignment is given by

$$i_x=I_x-I_{x,\mathrm{ref}}$$

and the Routhian by

$$e'=E-\hbar\omega I_x+\hbar\int I_{x,\mathrm{ref}}d\omega\ .$$

In the preceding equations, I_x is the projection of the total spin on the rotation axis given semiclassically as

$$I_x=[(I+1/2)^2-K^2]^{1/2}\ ,$$

with $K=\sum\Omega$, and $I_{x,\mathrm{ref}}$ is a reference based on a frequency-dependent moment of inertia

$$\mathcal{J}_{\mathrm{ref}}=\mathcal{J}_0+\omega^2\mathcal{J}_1\ .$$

The Harris parameters[23] $\mathcal{J}_0=14.7\hbar^2$ MeV^{-1} and $\mathcal{J}_1=45.8\hbar^4$ MeV^{-3} have been obtained from a fit of the expression

$$I_x=\omega(\mathcal{J}_0+\omega^2\mathcal{J}_1)+i_x$$

to states of the yrast band 7 below $\hbar\omega=0.43$ MeV.

A. CSM calculations

In order to compare the experimental results with theoretical predictions, cranked shell model calculations have been carried out using a Nilsson potential with the parameters κ and μ taken from Ref. 24. The pairing gap Δ has been set to 1.2 MeV for both protons and neutrons, and the chemical potential λ has been adjusted to reproduce the particle numbers at zero rotational frequency. A quadrupole deformation $\epsilon_2=0.2$ and a hexadecapole

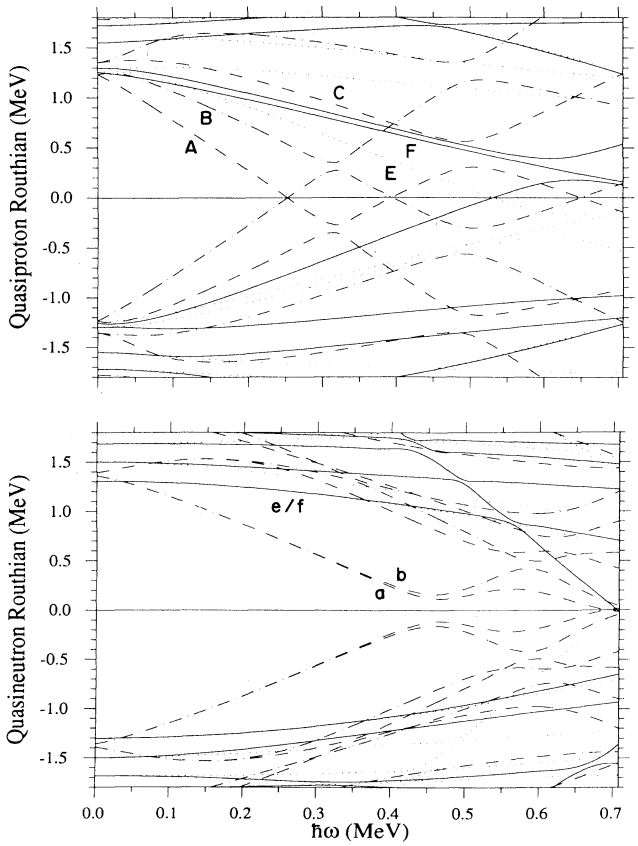

FIG. 4. Cranked shell model calculations for ^{131}La. Quasiparticle energies for protons (top) and neutrons (bottom) as a function of rotational frequency ($\hbar\omega$). The parameters used are $\epsilon_2=0.2$, $\epsilon_4=0.0$, $\gamma=0°$, and $\Delta_p=\Delta_n=1.2$ MeV. Solid lines correspond to $(\pi,\alpha)=(+,+\frac{1}{2})$; dotted lines to $(+,-\frac{1}{2})$; dash-dotted lines to $(-,+\frac{1}{2})$; and dashed lines to $(-,-\frac{1}{2})$.

TABLE III. Labeling of quasiparticle orbitals adopted in this paper. Shell model states and Nilsson quantum numbers (for $\hbar\omega=0$, axial) are also shown.

Shell model state	Nilsson orbital	Signature component	Quasiparticle label
$\pi h_{11/2}$	$\frac{1}{2}^-[550]$	$\alpha=-\frac{1}{2}$	$[A]$
		$\alpha=+\frac{1}{2}$	$[B]$
$\pi h_{11/2}$	$\frac{3}{2}^-[541]$	$\alpha=-\frac{1}{2}$	$[C]$
		$\alpha=+\frac{1}{2}$	$[D]$
$\pi g_{7/2}$	$\frac{5}{2}^+[413]$	$\alpha=-\frac{1}{2}$	$[E]$
		$\alpha=+\frac{1}{2}$	$[F]$
$\pi d_{5/2}$	$\frac{3}{2}^+[411]$	$\alpha=+\frac{1}{2}$[a]	$[G]$
		$\alpha=-\frac{1}{2}$	$[H]$
$\nu h_{11/2}$	$\frac{9}{2}^-[514]$	$\alpha=-\frac{1}{2}$	$[a]$
		$\alpha=+\frac{1}{2}$	$[b]$
$\nu h_{11/2}$	$\frac{7}{2}^-[523]$	$\alpha=-\frac{1}{2}$	$[c]$
		$\alpha=+\frac{1}{2}$	$[d]$
$\nu g_{7/2}$	$\frac{7}{2}^+[404]$	$\alpha=-\frac{1}{2}$	$[e]$
		$\alpha=+\frac{1}{2}$	$[f]$

[a]For the $\pi d_{5/2}$ orbital, $\alpha=+\frac{1}{2}$ is the favored signature component; for the other orbitals, $\alpha=-\frac{1}{2}$ is the favored component.

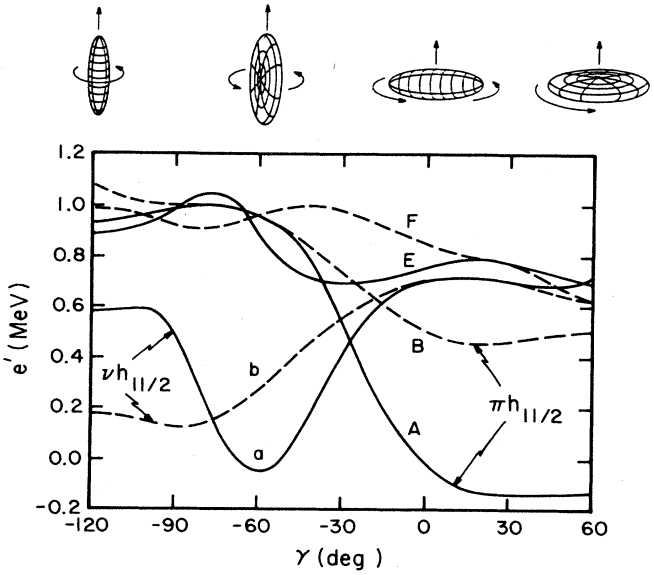

FIG. 5. Calculated single-quasiparticle levels in ^{131}La shown as a function of the γ deformation. The shape and sense of rotation of the nucleus is indicated at the top of the figure for specific values of γ that correspond to axially symmetric shapes. The calculation performed at a frequency $\hbar\omega=250$ keV, with $\epsilon_2=0.2$, $\epsilon_4=0$, and $\Delta_n=\Delta_p=1.2$ MeV.

deformation $\epsilon_4=0.0$ were used throughout the calculations. Small changes in ϵ_2 and ϵ_4 do not significantly change the results. The calculated quasiparticle Routhians for a prolate symmetric rotor ($\gamma=0°$) are shown in Fig. 4 as a function of rotational frequency. The Nilsson labels for the orbitals at zero rotational frequency are listed in Table III. The negative- (positive-) parity proton orbitals are labeled $[A],[B],[C],\ldots$ ($[E],[F],[G],\ldots$), while the negative- (positive-) parity neutron orbitals are similarly labeled $[a],[b],[c],\ldots$ ($[e],[f],[g]\ldots$). In this notation, band crossings are labeled by the quasiparticles that align. Thus, the first $\pi h_{11/2}$ alignment is labeled as the $[AB]$ crossing, while the second $\pi h_{11/2}$ alignment is labeled as the $[BC]$ crossing. The shell-model configurations for the bands numbered 1–15 and shown in Figs. 2(a) and 2(b) are listed in Table IV.

TABLE IV. Possible configurations for most of the bands of ^{131}La as shown in Figs. 2(a) and (b). Two configurations are given for the strongly coupled $\Delta I=1$ bands where the signature splitting is small.

Band number[a]	Shell-model configuration	Quasiparticle configuration
1	$\pi d_{5/2}$	$[G]$
2	$\pi d_{5/2}$	$[H]$
3	$\pi g_{7/2}$	$[F]$
4	$\pi g_{7/2}$	$[E]$
5	$\pi g_{7/2}\otimes[\pi h_{11/2}]^2$	$[EAB]$
6	$\pi g_{7/2}\otimes[\pi h_{11/2}]^2$	$[FAB]$
7	$\pi h_{11/2}$	$[A]$
8	$\pi h_{11/2}$	$[B]$
9	($\pi h_{11/2}\otimes\gamma$ vibrational)	($\gamma-[A]$)
10	($\pi h_{11/2}\otimes\gamma$ vibrational)	($\gamma-[B]$)
11		
12	$\pi g_{7/2}\otimes\nu h_{11/2}\otimes\nu g_{7/2}$	$[Eae],[Fae]$
13	$\pi h_{11/2}\otimes[\nu h_{11/2}]^2$	$[Aab],[Bab]$
14		
15	$\pi g_{7/2}\otimes[\nu h_{11/2}]^2$	$[Eab],[Fab]$

[a]The band numbers refer to the labels in Figs. 2(a) and (b).

Since, in this mass region, the nuclear shape is expected to be soft with respect to the triaxial deformation, the quasiparticle orbitals have also been calculated for different values of the shape asymmetry parameter γ. The results of such a calculation are presented in Fig. 5 where the quasiparticle energies for the proton orbitals $[A]$, $[B]$, $[E]$, and $[F]$, and the neutron orbitals $[a]$ and $[b]$ are plotted as a function of γ. The calculation was performed at a fixed rotational frequency $\hbar\omega=0.25$ MeV. As can be seen, the proton orbitals $[A]$ and $[B]$ have a strong driving force on the nuclear shape towards $\gamma\geq 0°$, whereas the neutron orbitals $[a]$ and $[b]$ favor an oblate shape with $\gamma\sim -60°$. The positive-parity orbitals $[E]$ and $[F]$ do not have such a strong dependence on the γ deformation, as is the case with the positive-parity neutron orbitals.

B. The prolate bands

For the yrast band-7, the experimental Routhian is best reproduced in the calculations by the orbital $[A]$ in Fig. 4, assuming a prolate ($\gamma=0°$) deformation. This orbital is the $\alpha=-\frac{1}{2}$ signature component of the $\frac{1}{2}^-[550]$ Nilsson orbital originating from the $h_{11/2}$ proton subshell. The $\alpha=+\frac{1}{2}$ signature component (labeled $[B]$ in

Fig. 4) is expected to be higher in excitation energy. Band 8, starting at 906 keV, is an obvious candidate for the band built on this unfavored state. Moreover, the alignment of this band ($i_x = 3.8\hbar$) is close to that of the yrast band ($i_x = 4.2\hbar$). The signature splitting of these bands (energy difference between the $\alpha = \pm\frac{1}{2}$ signature components) at $\hbar\omega = 0.25$ MeV is found to be $\Delta e' = 450$ keV, which is in good agreement with the predicted value of $\Delta e' \sim 500$ keV for a near-prolate shape (see Fig. 5).

The predicted $[AB]$ proton crossing at a rotational frequency $\hbar\omega = 0.31$ MeV is not observed in these two bands since either orbital $[A]$ or $[B]$ is occupied, which thus blocks the crossing. At higher rotational frequencies, an upbend is observed in band $[A]$ at $\hbar\omega_c = 0.54$ MeV. The corresponding band in the ^{133}Pr isotone[20] has an upbend at $\hbar\omega_c = 0.43$ MeV, thereby indicating a strong dependence of the band crossing frequency with proton number. A comparison with the isotopes ^{127,129}La ($\hbar\omega_c = 0.50$ MeV and $\hbar\omega_c = 0.57$ MeV, respectively)[21] shows a less dramatic change with decreasing neutron number. Assuming a prolate nuclear shape, this implies a proton origin for the upbend. The calculations of Fig. 4 predict the $[BC]$ proton crossing at $\hbar\omega_c = 0.51$ MeV, close to the experimental value. However, $h_{11/2}$ neutrons are also expected to align (the $[ab]$ crossing) close to this rotational frequency, and hence no definite conclusion can be drawn.

The favored band 7 is expected, from Fig. 5, to have a shape with $\gamma \geq 0°$. This is because of the strong γ-driving force of the $[A]$ $h_{11/2}$ proton orbital. The orbital $[B]$ does not have an equally strong γ-driving effect, and the unfavored band 8 is therefore more influenced by the shape of the core. Since the nuclear core has the largest moment of inertia for a triaxial shape with $\gamma = -30°$ (Ref. 1), it will strive to adopt this shape when the rotational frequency increases. This leads to a decrease in the Routhian e' and therefore an upbend in the alignment plot. The effect will be more pronounced in the unfavored and less γ-driving band $[B]$ and could partly be an explanation for the upbend observed in band 8. The favored and unfavored signature components of the $h_{11/2}$ proton band can thus have different γ deformations. The neutron $[ab]$ alignment frequency is then expected to be different in the favored and unfavored bands because of a difference in shape. The neutron alignment frequency decreases as γ moves to more negative values and will thus occur earlier in band $[B]$.

The positive parity bands 1–4 all have similar Routhians and alignments. Their configurations are expected to be based on the $\frac{5}{2}^+[413]$ and $\frac{3}{2}^+[411]$ Nilsson orbitals that originate from admixtures of states from the $g_{7/2}$ and $d_{5/2}$ proton shells. The small signature splitting between bands 3 and 4 is indicative of a strongly coupled particle (high Ω). Since the $\alpha = -\frac{1}{2}$ signature is the favored component, the configuration must be dominated by the $g_{7/2}$ proton. For a $d_{5/2}$ particle, the $\alpha = +\frac{1}{2}$ component is expected to be lower in energy. Band 1 can therefore be associated with this configuration and band 2, based on the $\frac{3}{2}^+$ ground state, is the unfavored ($\alpha = -\frac{1}{2}$) component.

In the CSM calculations the orbitals $[E]$, $[F]$, $[G]$, and $[H]$ correspond to bands 4, 3, 1, and 2, respectively. The calculations reproduce the main features of the positive-parity orbitals although there is a difference between the predicted and the experimentally observed signature splittings. This is probably a consequence of the bands not having a prolate symmetric shape. When considering a triaxial deformation with the same value of γ for all four bands, there are still some discrepancies. It is therefore likely that the bands have different minima in the (β, γ) plane, and somewhat different shapes.

Bands 5 and 6, which feed into the yrast band, are most likely based on both signature components of a three-quasiparticle configuration. The alignment of $i_x \sim 8.5\hbar$ for these bands indicates that two $h_{11/2}$ particles are involved and, as for the isotone ^{133}Pr, we have adopted the $\pi g_{7/2} \otimes [\pi h_{11/2}]^2$ configuration for these bands. Following the notations of Table III, these bands correspond to the $[EAB]$ and $[FAB]$ configurations, respectively. These three-quasiparticle bands cross the one-quasiparticle $[E]$ and $[F]$ bands (bands 3 and 4) at $\hbar\omega_c = 0.315$ MeV, thus defining the $[AB]h_{11/2}$ proton crossing frequency. This proton crossing is close to the predicted crossing frequency in Fig. 4. The alignment gain at the crossing is close to the sum of the alignments for the individual orbitals $[A]$ and $[B]$. The signature splitting between the two components decreases with increasing rotational frequency and becomes zero at $\hbar\omega = 0.43$ MeV. In the CSM calculation, a zero splitting between the orbitals $[E]$ and $[F]$ is predicted to occur for $\gamma > 0°$ (see Fig. 5). The observed decrease in the splitting can then be explained by the strong driving force of the $h_{11/2}$ protons which will give the nucleus a deformation with $\gamma \geq 0°$. The lack of transitions connecting bands 3 and 4 with bands 5 and 6 could be a consequence of the bands having somewhat different triaxial shapes.

There is an additional indication of a band crossing in bands 3 and 4 at $\hbar\omega_c \sim 0.4$ MeV. The gain in alignment of at least $7\hbar$ again points to an alignment of a pair of $h_{11/2}$ quasiparticles. The proton $[BC]$ and $[AD]$ crossings are predicted at $\hbar\omega_c = 0.5$ MeV, which is too high in rotational frequency to explain the crossing. The neutron $[ab]$ crossing, predicted to occur at $\hbar\omega_c = 0.46$ MeV, is more likely. If the nucleus has a small negative γ deformation, the neutron crossing frequency will decrease and will then come closer to the observed value. Band crossings at similar rotational frequencies have been observed in the even-even ^{128,130}Ba nuclei ($\hbar\omega_c = 0.43$ MeV and 0.40 MeV, respectively) and have been attributed to the breakup and alignment of an $h_{11/2}$ neutron pair.[25,26] When moving away from a prolate shape to negative γ values, the splitting between the $[E]$ and $[F]$ orbitals increases. For this reason, it is only the favored band that can be followed up to a sufficiently high spin to clearly see the backbend. When fully aligned, the neutrons will induce a shape change towards large negative γ values ($\gamma = -60°$). The aligned three-quasiparticle bands, based on the $\pi g_{7/2} \otimes [\nu h_{11/2}]^2$ configuration, and the corresponding one-quasiparticle bands ($\pi g_{7/2}$) will then have large differences in shape. This is expected to give a small interaction between the bands, which partly can ex-

plain why the bands are not observed above the crossing. Possible candidates for the [*Eab*] and [*Fab*] configurations with oblate shapes are discussed in Sec. IV D.

A definite interpretation for the $\Delta I=2$ bands 9 and 10, which are of negative parity, has not been made. The only negative-parity proton orbitals at this Fermi level involve the $h_{11/2}$ spin-orbit intruder. Bands built on the [*C*] and [*D*] $\pi h_{11/2}$ orbitals are expected at somewhat higher energy and will not be near yrast. Furthermore, with the proton in the [*C*] or [*D*] orbitals, the [*AB*] crossing is no longer blocked and should occur at $\hbar\omega\sim 0.31$ MeV. However, this crossing is not observed in bands 9 and 10. The high-Ω oblate $\frac{11}{2}^-[505]$ orbital, however, could result in a separate negative-parity band. This oblate high-Ω orbital is predicted[27] to achieve low energies for nuclei with proton numbers $Z=53-57$. Bands associated with high-Ω orbitals, however, are expected to be strongly coupled $\Delta I=1$ bands with no signature splitting and strong $M1$ transitions. Bands 9 and 10 do not show these specific characteristics. It is possible that the unfavored signatures of the high-Ω and low-Ω orbitals, the latter of which is signature split, could interact because of similar I^π energies to alter this interpretation.

Alternatively, other collective modes can be invoked to describe bands 9 and 10. When considering the even-even neighbors ^{130}Ba and ^{132}Ce, rotational bands exist built on the 2^+_γ γ-vibrational states at 907-keV (Ref. 26) and 821-keV (Ref. 28) excitation energy, respectively. The γ-vibrational bands of neighboring even-even nuclei typically show strong $E2$ strength into the yrast band at each level competing with the in-band decay. Bands 9 and 10, showing similar decay properties, could therefore be based on the $h_{11/2}$ proton band coupled to the γ-vibrational band of the core. The excitation energy of the $\frac{15}{2}^-$ state above the $\frac{11}{2}^-$ isomer of 1053 keV is somewhat higher than the corresponding values for the 2^+_γ states in the even-even nuclei. This could be an effect of the $h_{11/2}$ proton stabilizing the nuclear shape around $\gamma=0°$. Similar bands to band 9, showing the same characteristic decay pattern, have systematically been observed in $_{53}$I, $_{55}$Cs (Ref. 29), and $_{59}$Pr (Ref. 20) isotopes.

C. Collective oblate band

Band 13 in Fig. 2(b) has several properties that are markedly different from the bands discussed so far. This band has strong $\Delta I=1$ transitions compared to the $E2$ crossovers with negative $E2/M1$ mixing ratios δ for the $\Delta I=1$ transitions. It also has a large constant alignment and no signature splitting. Although the parity of this band has not been experimentally determined, the above-mentioned properties point to a unique three-quasiparticle structure for this band, namely the negative parity $\pi h_{11/2}\otimes[\nu h_{11/2}]^2$ configuration.

In order to discuss the alignment for band 13, it should be noted that this band has an effective dynamic moment of inertia that is lower than those of the other bands. This is illustrated in Fig. 6 where $\mathcal{J}^{(2)}_{\rm eff}=dI_x/d\omega$ is plotted for the yrast band and band 13 as a function of rotational

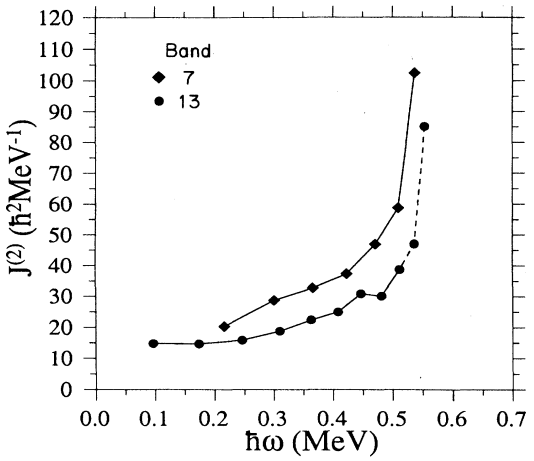

FIG. 6. Dynamic moment of inertia for the $\pi h_{11/2}$ band 7 (diamonds) and the oblate $\pi h_{11/2}\otimes[\nu h_{11/2}]^2$ band 13 (circles).

frequency. The difference between the bands is indicative of different collective shapes. A reduction of $\sim 33\%$ is observed for band 13 and consequently, when extracting the alignment i_x, the reference moment of inertia has been reduced by the same amount. The alignment obtained in this way, when using $K=\frac{11}{2}$ (see below) and $I=\frac{19}{2}$ for the bandhead, is plotted in Fig. 3(c). It has a constant value $i_x=8.9\hbar$ over a large frequency range. The large alignment implies the presence of two decoupled $h_{11/2}$ particles. It is only at the highest rotational frequencies ($\hbar\omega\sim 0.55$ MeV) that an upbend is observed.

The experimental Routhians for the two signature components of band 13, plotted in Fig. 3(c), show no signature splitting. The absence of signature splitting can be explained from an investigation of Fig. 5. When the γ deformation changes from 0° to −60° (from a prolate to an oblate shape), the splitting between the $h_{11/2}$ proton [*A*] and [*B*] orbitals decreases from a large value to zero. The shape change is induced by the decoupling and rotational alignment of a γ-driving $h_{11/2}$ neutron pair; the orbitals [*a*] and [*b*] have energy minima close to $\gamma=-60°$. For such an oblate shape, the proton occupies the $\frac{11}{2}^-[505]$ Nilsson orbital and will be strongly coupled; the $\pi h_{11/2}\otimes[\nu h_{11/2}]^2$ configuration will thus possess a large K value of $\frac{11}{2}$.

The constant alignment of $8.9\hbar$ is close to the expected value for two fully decoupled $h_{11/2}$ neutrons. The proton in the proposed configuration is strongly coupled and does not contribute significantly to the alignment. Furthermore, for an oblate shape no proton alignment is expected below $\hbar\omega=0.57$ MeV, and since the neutron orbitals [*a*] and [*b*] are occupied, the first allowed neutron alignment is the [*cd*] crossing that is expected at $\hbar\omega\sim 0.6$ MeV.

To understand better the total energy of the valence nucleons and how the signature splitting depends on the triaxial deformation γ, total Routhians have been calculated using the expression[1]

$$E'(\gamma)=\sum e'(\gamma)+\tfrac{1}{2}V_{\rm PO}\cos 3\gamma-\tfrac{1}{2}(\hbar\omega)^2\mathcal{J}$$

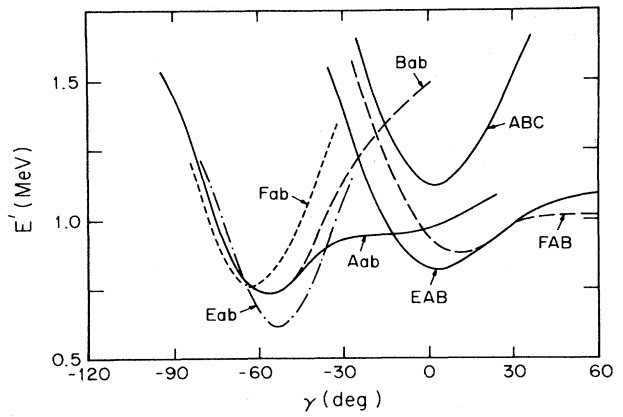

FIG. 7. Total Routhians for some selected one- and three-quasiparticle configurations in ^{131}La as a function of the γ deformation. The calculation was performed at $\hbar\omega=0.25$ MeV with $V_{\rm PO}$ set to zero.

at a fixed rotational frequency $\hbar\omega=0.25$ MeV. Here, $e'(\gamma)$ are the quasiparticle energies as a function of γ as shown in Fig. 5, and $V_{\rm PO}$ is the prolate-oblate energy difference. The reference moment of inertia $\mathcal{J}$ is given by the Harris expression multiplied by a hydrodynamical γ dependence:

$$\mathcal{J}=(\mathcal{J}_0+\tfrac{1}{2}\omega^2\mathcal{J}_1)\tfrac{4}{3}\cos^2(\gamma+30^\circ)\ .$$

The results are presented in Fig. 7 where $V_{\rm PO}$ has been set to zero, i.e., assuming the prolate and oblate core potential energies are similar. As can be seen, a minimum occurs in the total Routhians at $\gamma=-60^\circ$ for the negative-parity [*Aab*] and [*Bab*] configurations ($\pi h_{11/2}\otimes[\nu h_{11/2}]^2$). It is clear that only the [*Aab*] and [*Bab*] configurations have zero signature splitting at the predicted minimum, namely for $\gamma\sim-60^\circ$. The positive-parity configurations [*Eab*] and [*Fab*] ($\pi g_{7/2}\otimes[\nu h_{11/2}]^2$) are also seen to decrease in energy for an oblate shape. However, these configurations cannot explain band 13 because of the predicted signature splitting of $\sim$150 keV contrary to the experimental value for this band ($\Delta e'\sim0$). The experimentally deduced Routhian, signature splitting and alignment of band 13 are thus consistent with the negative-parity configuration having an oblate $\pi h_{11/2}\otimes[\nu h_{11/2}]^2$ configuration.

The data do not give a direct measurement of the difference in the total energy between prolate and oblate shapes. An estimate of $V_{\rm PO}$, however, may be obtained from the experimental Routhians when extrapolated down to zero rotational frequency. At this point, the energy difference between different orbitals does not depend on any reference moment of inertia and is given by the quantity

$$2\Delta_n-V_{\rm PO}\ ,$$

where Δ_n is the neutron pairing gap including the residual neutron-proton and neutron-neutron interactions. The oblate band and the prolate $\pi h_{11/2}$ band have, when extrapolated down to $\hbar\omega=0$, an energy difference of 2.3 MeV. Assuming the neutron pair gap $\Delta_n\geq1.0$ MeV (a smaller value seems unrealistic and results in the [*ab*] neutron crossing occurring below 0.4 MeV, contrary to the observed alignments in the positive parity [*E*] and [*F*] bands), then a value $V_{\rm PO}\geq-300$ keV is obtained. Since the prolate shape is favored over the oblate shape, $V_{\rm PO}$ cannot be positive. Thus, an estimate for $V_{\rm PO}$ at zero rotational frequency of $0\geq V_{\rm PO}\geq-300$ keV is obtained for ^{131}La which is in good agreement with the theoretical predictions of Refs. 3 and 9.

Finally, band 13 shows very little interaction with other structures in this nucleus. The decay out of the band goes through several branches and feeds mainly the $(\frac{17}{2}^+)$ state of band 15 and the $\frac{21}{2}^-$ isomeric state of band 12. No transitions were observed that directly connected band 13 with the prolate deformed bands, indicating a weak interaction between the bands that is most likely due to the difference in shape. The interaction must be smaller than the energy difference between the states of the same spin and parity (assuming that there are only two such states). With the proposed spin assignments, the $\frac{29}{2}^-$ states of the oblate band 13 and the unfavored band [*B*] are separated by about 75 keV.

D. Other structures in ^{131}La

There are additional structures in ^{131}La above an excitation energy of 2.0 MeV that were only populated weakly and could not be studied in detail. No definite configuration assignment, therefore, could be made. For example, there exists an isomeric level at 2121 keV, from which the main decay directly feeds the yrast $\pi h_{11/2}$ band via a 947.6-keV transition. The 38-ns half-life is indicative or a significantly different structure or shape between the isomer and the prolate yrast band. There are transitions observed feeding the isomer (band 12). The relatively strong $\Delta I=1$ transitions compared to the $E2$ crossovers and the regular increase of the transition energies with spin imply a rotational band based on a high-K configuration. Using $K=\frac{21}{2}$, an alignment close to $2\hbar$ is obtained. Negative parity bands with similar alignments, based on high-K isomers, have been found in the neighboring isotopes ^{128}Ba (Ref. 30) and ^{130}Ce (Ref. 31) with a proposed $\nu g_{7/2}\otimes\nu h_{11/2}$ neutron configuration. It is possible that band 12 in ^{131}La has the odd proton coupled to this configuration, namely, band 12 is built on the $\pi g_{7/2}\otimes\nu g_{7/2}\otimes\nu h_{11/2}$ configuration. The shape of the band built on this configuration would be dominated by the $[a]\nu h_{11/2}$ orbital. Thus, an oblate $\gamma\sim-60^\circ$ shape is expected, which would explain both the strong connection to the oblate band 13 and the isomeric decay to the prolate band 7. Following the notations of Table III, band 12 would then be built on the [*Eae*] and [*Fae*] configurations.

Band 15, with the proposed bandhead of $I^\pi=\frac{17}{2}^+$ at 2345 keV, shows no well-developed rotational structure. The excitation energy and the level spacings within the band are close to those found for a band based on a $\frac{17}{2}^{(+)}$ state at 2368 keV in ^{133}La (Ref. 19). An assignment of a

similar configuration for the two bands is plausible, and for ^{133}La a $d_{5/2}$ or $g_{7/2}$ proton weakly coupled to noncollective states in the even-even core was proposed.[32] An alternative interpretation is in terms of an oblate band similar to the more strongly populated band 13 ([*Aab*] and [*Bab*]), and, perhaps, band 12 ([*Eae*] and [*Fae*]). The level spacings within band 15 increase with excitation energy, although an energy staggering effect seems to be present. A possible configuration for the band is the $\pi g_{7/2}\otimes[\nu h_{11/2}]^2$ configuration with signature components [*Eab*] and [*Fab*]. These two components come low in energy for $\gamma\sim-60°$ (see Fig. 7) and their signature splitting would explain the energy staggering.

The structure starting at 3580 keV [band 11 in Fig. 2(b)] may also have a counterpart in ^{133}La, where a $(\frac{27}{2})$ state is known at 3599 keV. Here the $h_{11/2}$ proton may be weakly coupled to noncollective excitations of the even-even core.

V. ELECTROMAGNETIC PROPERTIES

A. $B(M1)/B(E2)$ ratios

From the intensities of competing $\Delta I=1$ and $\Delta I=2$ transitions, it is possible to extract values for the ratios of the reduced transition rates for specific quasiparticle configurations using the approximate expression

$$\frac{B(M1;I\to I-1)}{B(E2;I\to I-2)}=0.693\times\frac{I_\gamma(M1)}{I_\gamma(E2)}\times\frac{E_\gamma^5(E2)}{E_\gamma^3(M1)}\ ,$$

where the $E2/M1$ mixing ratio for the $\Delta I=1$ transitions has been set to zero. Experimental values for such ratios have been extracted for transitions in the $\pi g_{7/2}$, $\pi g_{7/2}\otimes[\pi h_{11/2}]^2$, and the oblate $\pi h_{11/2}\otimes[\nu h_{11/2}]^2$ bands. The results are presented in Fig. 8 together with theoretical calculations obtained from a semiclassical formula,[33,34]

$$\frac{B(M1;I\to I-1)}{B(E2;I\to I-2)}=\frac{12}{5Q_0^2\cos^2(\gamma+30°)}\times\left[1-\frac{K^2}{(I-\frac{1}{2})^2}\right]^{-2}\frac{K^2}{I^2}\times\{(g_1-g_R)[(I^2-K^2)^{1/2}-i_1]-(g_2-g_R)i_2\}^2\left[1\pm\frac{\Delta e'}{\hbar\omega}\right]^2\ ,$$

where a signature dependent term has been included. Here g_1 and i_1 are the gyromagnetic factor and alignment for the strongly coupled quasiparticle, while g_2 and i_2 refer to the gyromagnetic factor and alignment of the decoupled quasiparticles. The rotational gyromagnetic factor g_R was taken as $Z/A=0.435$, and empirical values, taken from nearby nuclei, were used for the g factors of the quasiparticles. The quadrupole moment was calculated assuming a deformation parameter $\beta=0.2$.

For the $\pi g_{7/2}$ band, the experimental values of the $B(M1)/B(E2)$ ratios show an increase with increasing spin. There is also a marked signature dependence that is more strongly pronounced in the data than in the model calculations. Above the $[\pi h_{11/2}]^2$ proton alignment, the ratios of the reduced transition rates remain constant at a value that is slightly lower than those below the crossing. Model calculations for both pure $\pi d_{5/2}\otimes[\pi h_{11/2}]^2$ and $\pi g_{7/2}\otimes[\pi h_{11/2}]^2$ configurations are also shown. The decrease of the ratio above the crossing can be seen as an effect of the aligned $h_{11/2}$ protons. When a quasiparticle pair align, the term $(g_2-g_R)i_2$ is introduced in the formula; for $h_{11/2}$ protons, which have positive g factors, this term tends to cancel the contribution from the other strongly coupled quasiparticle ($\pi g_{7/2}$ or $\pi d_{5/2}$), which also has a positive g factor.

The extracted $B(M1)/B(E2)$ ratios for the oblate band 13 are more than an order of magnitude larger than those of the prolate one- and three-quasiproton bands. This can only be quantitatively reproduced in the model calculations when using the proposed oblate $\pi h_{11/2}\otimes[\nu h_{11/2}]^2$ configuration with $K=\frac{11}{2}$. The larger values for the ratios result for two reasons. First, whereas the $[\pi h_{11/2}]^2$ proton alignment introduces a cancellation into the $B(M1;I\to I-1)$ expression, a $[\nu h_{11/2}]^2$ neutron alignment causes an enhancement because of the negative sign of the g factor. Secondly, the reduced $M1$ transition probability is proportional to the square of $\mu_\perp$, the component of the magnetic dipole moment perpendicular to the total spin **I** of the nucleus. For high K, this component will be large and thus the $B(M1)$ values will be enhanced. It is only for an oblate shape ($\gamma=-60°$) that a proton orbital of sufficiently high Ω comes close to the Fermi surface, namely the $\Omega=\frac{11}{2}$

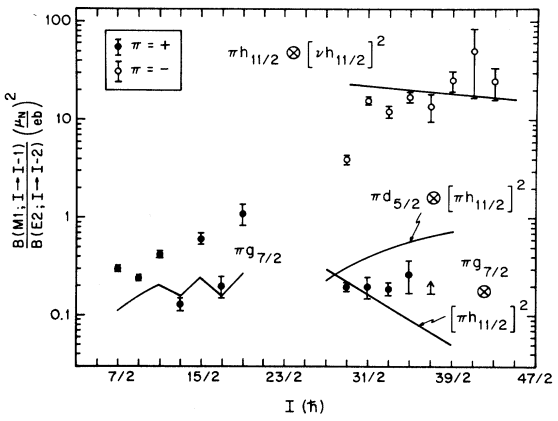

FIG. 8. Ratios of reduced transition probabilities $B(M1)/B(E2)$ extracted for the positive-parity bands 3,4 and 5,6 and the oblate band 13. The lines represent calculations for the given pure configurations using the geometrical model of Dönau and Frauendorf (Ref. 33).

member of the proton $h_{11/2}$ shell ($\frac{11}{2}^-[505]$). Thus the oblate $\pi h_{11/2}\otimes[\nu h_{11/2}]^2$ configuration will possess high K and the $B(M1)/B(E2)$ ratios will be correspondingly large. Other possible configurations for band 13 involving a strongly coupled $g_{7/2}$ or $d_{5/2}$ proton together with the aligned $h_{11/2}$ neutrons are predicted to have $B(M1)/B(E2)$ ratios four times smaller than the measured values for this band.

B. The mixing ratios

The $E2/M1$ mixing ratio δ for $\Delta I=1$ transitions can give additional information on the nuclear shapes. Using the semiclassical model,[33] Dönau and Frauendorf define a mixing ratio thus:

$$\delta_{\rm DF}=(\tfrac{5}{3})^{1/2}Q_0\cos(\gamma+30^\circ)\left[1-\frac{K^2}{I^2}\right]^{1/2}$$
$$\times\{(g_1-g_R)[(I^2-K^2)^{1/2}-i_1]-(g_2-g_R)i_2\}^{-1}\ ,$$

which is related to conventional experimental δ values[35] through the relationship

$$\delta=0.835\delta_{\rm DF}E_\gamma({\rm MeV})\ .$$

For the oblate band 13 with the proposed $\pi h_{11/2}\otimes[\nu h_{11/2}]^2$ configuration, the $M1$ contribution to the mixing ratio (the expression within the curly brackets) is positive and therefore $\mathrm{sgn}(Q_0)=\mathrm{sgn}(\delta)$. The large negative A_2/A_0 coefficients found for the $\Delta I=1$ transitions in this band imply negative mixing ratios and hence $Q_0<0$, namely an oblate shape ($\gamma=-60^\circ$). An estimate of the mixing ratios for the lower $\Delta I=1$ transitions, obtained from the angular distribution data, yields $-0.21\le\delta\le-0.07$, which is in qualitative agreement with calculations using the simplified model that predicts $\delta\sim-0.2$.

VI. SUMMARY

The odd-proton nucleus ^{131}La has been produced in compound nuclear reactions, and its γ decay has been studied revealing states up to high spin. The results have been interpreted within the framework of the cranked shell model including effects of the triaxial deformation γ. Bands based on prolate and oblate shapes, collectively rotating around an axis perpendicular to the symmetry axis, have been identified. These bands coexist in the nucleus over a large frequency range.

The yrast band is based on an $h_{11/2}$ proton decoupled from a prolate core. It was observed up to spin $I^\pi=(\frac{55}{2}^-)$ with an upbend at $\hbar\omega=0.54$ MeV. Both the second $h_{11/2}$ proton alignment, the $[BC]$ crossing (the $[AB]$ crossing is blocked), and the first $h_{11/2}$ neutron alignment, the $[ab]$ crossing, could be responsible for this effect. The unfavored signature partner of the yrast band was also identified with a large signature splitting with respect to the yrast band. Two additional bands with presumably negative parity were also established. Possible interpretations involve an oblate strongly coupled $\pi h_{11/2}$ orbital or an $h_{11/2}$ proton coupled to the γ-vibrational states of the core.

Four positive-parity bands were found at low excitation energy with small alignments and small signature splittings. These are one-quasiproton bands based on Nilsson orbitals arising from the $g_{7/2}$ and $d_{5/2}$ shells. At higher excitation energies, two positive-parity three-quasiproton bands were observed and assigned the $\pi g_{7/2}\otimes[\pi h_{11/2}]^2$ configuration. This assignment is based on systematics with other odd-Z isotopes in this mass region and is consistent with measured ratios of reduced transition probabilities $B(M1)/B(E2)$. The crossing with the corresponding one-quasiproton bands at $\hbar\omega=0.31$ MeV defines the $[AB]$ $h_{11/2}$ proton crossing frequency where the gain in the alignment is $\sim8\hbar$. The signature splitting between the three-quasiproton bands falls to zero with increasing spin, which may indicate that the nucleus is adopting a triaxial shape with small positive values of the triaxial deformation γ. Evidence for a second band crossing in two of the one-quasiproton bands was found at $\hbar\omega\sim0.4$ MeV, possibly due to the $[ab]h_{11/2}$ neutron alignment.

A strongly populated $\Delta I=1$ band was observed and assigned the $\pi h_{11/2}\otimes[\nu h_{11/2}]^2$ configuration with an oblate shape ($\gamma=-60^\circ$) that rotates collectively around an axis perpendicular to the symmetry axis. This band coexists with the other near-prolate bands. The assignment is based on the large values of the $B(M1)/B(E2)$ ratios, the lack of signature splitting, and the negative mixing ratios δ for the $\Delta I=1$ transitions. The constant alignment of $8.9\hbar$ over a large frequency range is consistent with this configuration. The band has only a weak interaction with the prolate bands as a consequence of the difference in shape.

Additional band structures were observed in ^{131}La, but no firm assignments could be made. Possible configurations for some of these bands are the $\pi g_{7/2}\otimes\nu g_{7/2}\otimes\nu h_{11/2}$ configuration for the $\frac{21}{2}^-$ isomeric state (band 12) and the $\pi g_{7/2}\otimes[\nu h_{11/2}]^2$ configuration with an oblate shape for the $(17/2^+)$ state (band 15).

The existence of collective bands of both prolate and oblate shapes in ^{131}La shows that this nucleus is soft with respect to γ, and its shape is strongly influenced by the excited valence quasiparticles. An estimate of the prolate-oblate energy difference at zero rotational frequency from the measured Routhians gives a limit $V_{\rm PO}\ge-300$ keV, i.e., the oblate minimum is higher in energy than the prolate minimum but by no more than 300 keV.

This work was supported in part by the National Science Foundation.

*Present address: Lawrence Berkeley Laboratory, University of California, Berkeley, CA 94720.

[1]S. Frauendorf and F. R. May, Phys. Lett. **125B**, 245 (1983).

[2]G. A. Leander, S. Frauendorf, and F. R. May, in *Proceedings of the Conference on High Angular Momentum Properties of Nuclei, Oak Ridge, 1982,* edited by N. R. Johnson (Harwood Academic, New York, 1983), p. 281.

[3]I. Ragnarsson, A. Sobiczewski, R. K. Sheline, S. E. Larsson, and B. Nerlo-Pomorska, Nucl. Phys. **A233**, 329 (1974).

[4]Y. S. Chen, S. Frauendorf, and G. A. Leander, Phys. Rev. C **28**, 2437 (1983).

[5]G. Andersson, S. E. Larsson, G. Leander, P. Möller, S. G. Nilsson, I. Ragnarsson, S. Åberg, R. Bengtsson, J. Dudek, B. Nerlo-Pomorska, K. Pomorski, and Z. Szymański, Nucl. Phys. **A268**, 205 (1976).

[6]R. Aryaeinejad, D. J. G. Love, A. H. Nelson, P. J. Nolan, P. J. Smith, D. M. Todd, and P. J. Twin, J. Phys. G **10**, 955 (1984).

[7]R. Ma, E. S. Paul, C. W. Beausang, S. Shi, N. Xu, and D. B. Fossan, Phys. Rev. C **36**, 2322 (1987).

[8]W. F. Piel, Jr., C. W. Beausang, D. B. Fossan, L. Hildingsson, and E. S. Paul, Phys. Rev. C **35**, 959 (1987).

[9]W. Nazarewicz and G. A. Leander (private communication); B. D. Kern, R. L. Mlekodaj, G. A. Leander, M. O. Kortelahti, E. F. Zganjar, R. A. Braga, R. W. Fink, C. P. Perez, W. Nazarewicz, and P. B. Semmes, Phys. Rev. C **36**, 1514 (1988).

[10]S. Ingelman, C. Ekström, M. Olsmats, and B. Wannberg, Phys. Scr. **7**, 24 (1973).

[11]M. A. Deleplanque, C. Gerschel, and N. Perrin, Nucl. Phys. **A207**, 565 (1973).

[12]T. W. Conlon, Nucl. Phys. **A213**, 445 (1973).

[13]W. Andrejtscheff, L. Zamick, N. A. Lebedev, K. M. Muminov, T. M. Muminov, and U. S. Salikhbaev, Nucl. Phys. **A368**, 45 (1981).

[14]F. S. Stephens, R. M. Diamond, J. R. Leigh, T. Kammuri, and K. Nakai, Phys. Rev. Lett. **29**, 438 (1972).

[15]J. R. Leigh, K. Nakai, K. H. Maier, F. Pülhofer, F. S. Stephens, and R. M. Diamond, Nucl. Phys. **A213**, 1 (1973).

[16]P. A. Butler, J. Meyer-Ter-Vehn, D. Ward, H. Bertschat, P. Colombani, R. M. Diamond, and F. S. Stephens, Phys. Lett. **56B**, 453 (1975).

[17]E. S. Paul, C. W. Beausang, D. B. Fossan, R. Ma, W. F. Piel, Jr., N. Xu, L. Hildingsson, and G. A. Leander, Phys. Rev. Lett. **58**, 984 (1987).

[18]L. Hildingsson, C. W. Beausang, D. B. Fossan, W. F. Piel, Jr., A. P. Byrne, and G. D. Dracoulis, Nucl. Instrum. Methods **A252**, 91 (1986).

[19]T. Morek, H. Beuscher, B. Bochev, D. R. Haenni, T. Kutsarova, R. M. Lieder, M. Müller-Veggian, and A. Neskakis, Nucl. Phys. **A391**, 269 (1982).

[20]L. Hildingsson, C. W. Beausang, D. B. Fossan, and W. F. Piel, Jr., Phys. Rev. C **37**, 985 (1988).

[21]P. J. Smith, D. J. Unwin, A. Kirwan, D. J. G. Love, A. H. Nelson, P. J. Nolan, D. M. Todd, and P. J. Twin, J. Phys. G **11**, 1271 (1985).

[22]R. Bengtsson and S. Frauendorf, Nucl. Phys. **A327**, 139 (1979).

[23]S. M. Harris, Phys. Rev. **138**, 509B (1965).

[24]T. Bengtsson and I. Ragnarsson, Nucl. Phys. **A436**, 14 (1985).

[25]H. Wolters, K. Schiffer, A. Gelberg, A. Dewald, J. Eberth, R. Reinhardt, K. O. Zell, P. von Brentano, D. Alber, H. Grawe, Z. Phys. A **328**, 15 (1987).

[26]Sun Xiangfu, D. Bazzacco, W. Gast, A. Gelberg, U. Kaup, A. Dewald, K. O. Zell, and P. von Brentano, Phys. Rev. C **28**, 1167 (1983).

[27]J. Y. Zhang (private communication).

[28]A. Kirwan, P. J. Bishop, D. J. G. Love, P. J. Nolan, D. J. Thornley, A. H. Nelson, P. J. Twin, A. Dewald, A. Gelberg, K. Schiffer, and K. O. Zell, University of Liverpool Annual Report 84/85, 1985.

[29]Y. Liang, D. B. Fossan, R. Ma, E. S. Paul, and N. Xu (unpublished).

[30]K. Schiffer, A. Dewald, A. Gelberg, R. Reinhardt, K. O. Zell, Sun Xiangfu, and P. von Brentano, Nucl. Phys. **A458**, 337 (1986).

[31]D. M. Todd, R. Aryaeinejad, D. J. G. Love, A. H. Nelson, P. J. Nolan, P. J. Smith, and P. J. Twin, J. Phys. G **10**, 1407 (1984).

[32]M. Müller-Veggian, H. Beuscher, D. R. Haenni, R. M. Lieder, and A. Neskakis, Nucl. Phys. **A417**, 189 (1984).

[33]F. Dönau and S. Frauendorf, in *Proceedings of the Conference on High Angular Momentum Properties of Nuclei, Oak Ridge, 1982,* edited by N. R. Johnson (Harwood Academic, New York, 1983), p. 143; F. Dönau, Niels Bohr Institute-Zentralinstitut für Kernforschung Report 85-36, 1985.

[34]A. J. Larabee, L. H. Courney, S. Frauendorf, L. L. Riedinger, J. C. Waddington, M. P. Fewell, N. R. Johnson, I. Y. Lee, and F. K. McGowan, Phys. Rev. C **29**, 1934 (1984).

[35]K. S. Krane, At. Data Nucl. Data Tables **16**, 384 (1975).